AIAA JOURNAL
Vol. 47, No. 11, November 2009

Toward Understanding and Optimizing Separation Control Using Microjets

Vikas Kumar* and Farrukh S. Alvi†
Florida A&M University and Florida State University, Tallahassee, Florida 32311

DOI: 10.2514/1.38868

Flow separation in engine inlets and diffuser ducts and over external aerodynamic surfaces such as wings can significantly compromise performance. In a previous experimental study, we demonstrated the value of microjets for separation control. In this paper, we significantly broaden the range of conditions and parameters to explore the effects of microjet control on the efficiency of separation control over a backward-facing ramp. The parameters explored include the following: the freestream velocity, the ramp angle of attack, and the microjet pressure, location, and injection angle. Detailed velocity field investigations and unsteady pressure measurements have been conducted to study the effect of flow control over this parametric space. The results indicate that, by activating the actuator arrays in the immediate vicinity of the separation location, the control efficiency can be greatly enhanced, reducing the actuator mass flow needed dramatically. By correlating the unsteady surface pressure measurements with the measured velocity field, we demonstrate that, at least in the present geometry, the unsteady pressure alone can be used to 1) detect separation and hence identify which actuator(s) to activate, and 2) estimate the effect of control on a separated flowfield. Finally, based on the response of the flowfield to actuation, we propose some simple scaling laws for detecting and implementing separation control.

Nomenclature

C_μ	=	steady momentum coefficient
d_{Mj}	=	microjet diameter
H	=	ramp height
$\dot{m}_{in}$	=	rate of mass flux supplied through microjets
N	=	number of microjets
P_{rms}	=	rms value for unsteady pressure
U_j	=	microjet velocity
U_∞	=	freestream velocity
w	=	width of the model
X_{Mj}	=	microjet location
X_s	=	separation location
X_T	=	unsteady pressure transducer location
δ	=	boundary-layer height
ρ_∞	=	freestream density
Ψ_P	=	$(P_{\mathrm{rms,baseline}} - P_{\mathrm{rms,control}})/P_{\mathrm{rms,baseline}}$
$\Psi_P(L)$	=	scaling factor for the effect of microjet location on P_{rms}
$\Psi_P(P)$	=	scaling factor for the effect of microjet pressure on P_{rms}
ω_z	=	streamwise vorticity

I. Introduction

FLOW separation and its control are of considerable interest both from fundamental fluid dynamics and practical perspectives. Flow separation occurs when fluid already decelerated by frictional forces is unable to overcome the increasing pressure forces when exposed to an adverse pressure gradient. It can lead to significant reductions in performance for both internal and external flows, such as lift loss, increase in drag, buffeting, and pressure recovery losses (in engine inlet and transmission ducts), among others. As an example, inlet ducts [1] used in a blended wing body [2] (BWB) configuration are located on the aft end to reduce the size of aircraft and to diminish radar signatures from the engines. In commercial aircraft, the use of these inlets makes the BWB aircraft significantly lighter with the additional advantage of a higher lift-to-drag ratio [3]. The placement of serpentine inlet ducts, however, requires ingestion of a thick boundary layer developed over the aircraft surface. This thick boundary layer is much more susceptible to separation when it encounters adverse pressure gradients in the inlet/diffuser ducts. The pressure loss due to this separation reduces the overall system efficiency. Moreover, flow distortion and unsteadiness created due to this separation can result in aerodynamic stall and surge of the compressor and the fan blades [4,5]. Therefore, it is highly desirable to avoid boundary-layer separation as it can significantly compromise the performance of aircraft propulsion systems.

Numerous techniques [6–20] have been explored to control flow separation. These range from the use of passive devices such as vortex generators in the form of vanes and bumps [11,12], etc., to the use of flexible walls [13], synthetic jets [7,14], and acoustic excitation [8,9] as active control devices. However, to date, the performance of most of these techniques has been somewhat limited, although work continues to further increase the efficiency of the more promising approaches [17,21–23]. For example, passive devices such as vortex generators have been found to be effective in controlling separation. However, they need to be optimized for their location, size, and other parameters for a wider range of operating conditions and may induce parasitic drag when not needed. As a result, active flow control devices have been suggested as an alternative control technique. Some of these active control devices, such as synthetic jets, have been explored by Amitay et al. [7] and Smith and Swift [14] for separation control. A comprehensive review of synthetic jets can be found in Glezer and Amitay [24].

Similar control devices (piezoelectric synthetic jets) were also employed by Jenkins et al. [25] over a Stratford ramp. Based on their results, Jenkins et al. concluded that synthetic jets did not have sufficient velocity/momentum to provide effective control. The use of flexible walls [13] has also been attempted for separation control; however, it adds mechanical complexity to the system. In addition, the system is dependent on the combination of the membrane tension

Presented as Paper 4879 at the 35th AIAA Fluid Dynamics Conference and Exhibit, Toronto, Ontario, 6–9 June 2005; received 31 May 2008; revision received 6 March 2009; accepted for publication 6 March 2009.

*Graduate Research Assistant, Florida Center for Advanced Aero-Propulsion, Department of Mechanical Engineering. Student Member AIAA.
†Professor, Florida Center for Advanced Aero-Propulsion, Department of Mechanical Engineering. Associate Fellow AIAA.

and strip spacing on the substrate, and control efficacy goes down if the natural frequency of the membrane coincides with the more energetic flexural modes, thereby limiting its application to a specific range of conditions. Historically, acoustic excitation devices used by Ahuja et al. [9] and Zaman et al. [8] showed some benefits. However, these studies were facility dependent [10] and, as such, are limited from a practical perspective. More recently, plasma actuators [15–17] have been employed for separation control. The cost and complexity involved in such mechanisms are, at present, relatively higher, and their application to date is mainly limited to low Reynolds numbers. As we will discuss in this paper, the use of high-speed microjets is a relatively simple and robust technique for controlling separation over a broad range of conditions. We will also examine ways to optimize the microjet parameters to achieve separation control, which may minimize cost.

The investigation, examining the nature of separation and the means to control it, was initiated several years ago at the Advanced Aero-Propulsion Laboratory located at the Florida State University. In this study, initially sponsored by NASA under the Ultra-Efficient Engine Technology program, strategically located microjets were used to control flow separation generated by adverse pressure gradients. Based on their success in other applications [26,27], their ability to produce high-momentum, high streamwise vorticity, and their relative simplicity and ease of implementation, we anticipated these microjet-based actuators to be effective in separation control. Initial results from this research have been discussed in Kumar and Alvi [28], in which we explored the effectiveness of microjets as an active flow control device for the control of the boundary-layer separation. As the results discussed in our previous paper indicate, microjets were very successful in controlling flow separation.

This paper presents more comprehensive results from this ongoing study, for which we have greatly expanded the parametric range over which microjet flow control has been examined. As subsequent results will show, through this study, we have significantly optimized the use of microjets, achieving separation control with mass flow rates that are substantially lower, by almost an order of magnitude in some cases, than those reported in Kumar and Alvi [28]. More detailed measurements, including the velocity field data, have also been obtained, with which we hope to obtain a better fundamental understanding of the effect of flow control on the flowfield dynamics. Furthermore, we investigate the unsteady surface pressure as a means of sensing the flow state and implementing appropriate microjet control accordingly. These results, including our approach to optimize the use of microjet actuators and the guidelines and scaling laws for their implementation in separation control applications, are described in this article.

II. Experimental Details

A. Test Model

The experiments were performed in a subsonic, closed-return wind tunnel with a maximum freestream velocity of about 70 m/s (in its present configuration) in a 0.6×0.6 m^2 test section [29]. A pitot-static probe was used to measure the inlet flow speed of the wind tunnel.

The geometry used for the test model is a simple diverging Stratford ramp; a picture of this model and its schematic are shown in Fig. 1. The diverging section of the ramp begins at $X = 0$ and is preceded by a flat section 0.55 m (21.5 in.) in length. In theory, the ramp profile produces a Stratford-like pressure gradient [30] when at

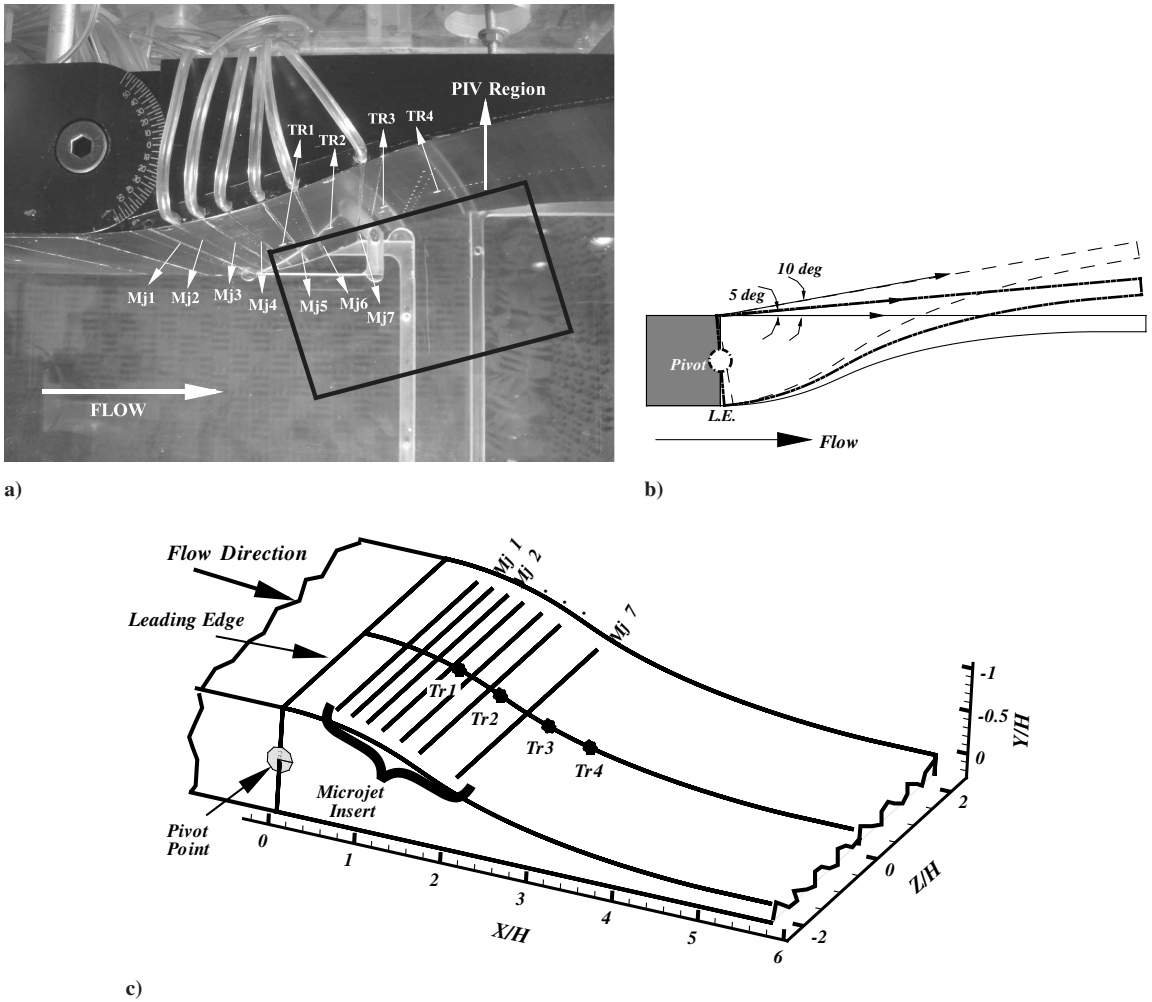

Fig. 1 Shown are the following: a) test model mounted in the test section, b) schematic of the angular ramp, and c) schematic of the test model.

a zero angle of attack (see Fig. 1b). At a zero angle of attack, the model profile is similar to a model used at NASA Langley Research Center, with which other separation control devices have been evaluated [25]. The model is designed to be highly adaptable, allowing us to change the base flow as well as the control parameters. For example, the ramp can be rotated about a pivot point providing the ability (see Fig. 1b) to change the adverse pressure gradient experienced by the flow, thereby controlling the nature (i.e., size and location) of the separated flow. Additionally, because the ramp is curvilinear in nature, it produces severe adverse pressure gradients at various locations reaching to a maximum slope of 34 deg (with respect to the freestream flow) for a 10 deg angle of attack. Figure 1a also indicates the region in which particle image velocity (PIV) measurements were conducted, discussed later in Sec. III.

The ramp is also equipped with seven linear arrays of microjets incorporated on a modular insert. The locations of these microjets, referred to as Mj1–Mj7, and the modular "microjet insert" are shown in Figs. 1a and 1c. This actuator insert contains seven slots for microjet modules in which different microjet modules, capable of supplying momentum at various angles with respect to the local flow, can be interchangeably deployed. In each array, the microjets are 400 μm in diameter with spacing of approximately 5 mm between microjets. The ramp is instrumented with more than 60 pressure taps along the centerline and in transverse arrays across the ramp at selected locations. In addition, the model is instrumented with four high-frequency-response pressure transducers for unsteady pressure measurement at selected locations. The placement of these pressure transducers (TR1–TR4 in Figs. 1a and 1c) was chosen to study the regions both upstream of and within the separation region; the location of the microjets and transducers is summarized in Table 1.

The microjets were supplied with "air" from compressed nitrogen tanks. Nitrogen was used because it is easily and cheaply available in pure form and has essentially the same gas dynamic properties as air.

B. Instrumentation, Hardware, and Measurement Uncertainties

Detailed PIV and unsteady pressure measurements were conducted to examine the flowfield and explore the possibility of using unsteady surface pressures as means of detecting separation. Mean pressure profiles were also obtained but are not discussed here as they are not pertinent to the focus of the present paper. Interested readers are referred to in Kumar [29].

To obtain whole-field velocity data in this flow, quantitative measurements were obtained using the two-component PIV, often referred to as 2-D PIV technique. Flow was seeded with smoke particles (1–10 μm) produced by a Rosco fluid fog generator. A New Wave Nd-YAG pulsed laser with an energy output of 200 mJ and a repetition rate of 15 Hz was used to illuminate the particles introduced into the flowfield. Each PIV image pair was then acquired using a Kodak ES1.0 high-resolution charge-coupled device camera capable of recording 10-bit digital image pairs in separate frames at a rate of 15 image pairs/second. Further details of this PIV technique can be found in Lourenco and Krothapalli [31]. One of the main advantages of this PIV technique is a processing scheme with high spatial resolution that uses image matching to extract the particle displacements and, hence, the velocities from particle image pairs [32]. An average of 1000 such images was used to obtain the ensemble-averaged velocity field. The boundary layer approaching the ramp was also measured using a boundary-layer pitot probe and was evaluated to be turbulent with a shape factor of 1.3.

Unsteady pressure measurements were made using high-frequency pressure Endevco® transducers with a resonant frequency at 55 kHz and a range of 0–1 psi. The pressure transducers were calibrated before each data acquisition. The signals through these transducers were filtered and amplified and a PC-based data acquisition system, using National Instruments software and hardware, was used to record the data.

The uncertainties associated with the unsteady pressure measurements, after taking into account the effects of linearity, hysteresis, repeatability, and the analog-to-digital converter resolution of the acquisition card, was estimated to be 0.03 psi. The freestream velocity measured using PIV was within 99% of that estimated using the pitot-static surveys. The uncertainty in the velocity field measurements after consideration of the error in particle displacement and the number of samples results in an error of 0.9 and 3.5% in the mean and the rms velocity, respectively, corresponding to a 95% confidence interval.

Table 1 Ramp configuration with a ramp height (H) of 57.2 mm (2.25 in.)

		Approximate locations (X/H)
Transducers	TR1	1.1
	TR2	1.6
	TR3	2.2
	TR4	2.7
Microjets	Mj2	0.7
	Mj3	0.9
	Mj4	1.0
	Mj5	1.3
	Mj6	1.5
	Mj7	1.9

C. Test Conditions

The experiments were conducted up to a maximum freestream velocity of 65 m/s. However, due to restrictions imposed by the cooling capacity of the heat exchanger in the wind tunnel, tests at 65 m/s were limited to shorter durations, limiting the parametric range of experiments at this velocity. As such, the most extensive studies of velocity and pressure field were conducted at a freestream velocity of 40 m/s (at which the tunnel can be operated in a continuous mode) at an angle of attack of 5 deg, which will be referred to as the primary test case (PTC) from hereon. This was chosen as the primary case as this flowfield contains the principal flow features and their response to microjet control. The conclusions drawn based on the PTC are generally applicable to the entire range of conditions.

The test conditions including the parameters for the baseline flow and the microjet control are provided in Table 2. Also included in the table are the boundary-layer integral parameters at the ramp leading edge for the PTC of 40 m/s. The Reynolds number at the leading edge of the ramp [corresponding to an upstream flat plate section of 0.55 m (21.5 in.)] for this case is 1.3×10^6. The boundary-layer profile obtained using a boundary-layer probe was in close agreement with the seventh power law profile (shape factor 1.3), indicating that the incoming boundary layer is nominally turbulent.

Appropriate measurements have been obtained at judiciously selected points within the aforementioned test envelope to examine the parametric effects of microjet control on the separated flow over the entire range of conditions.

Table 2 Test conditions and boundary layer parameters

Inlet flow conditions	
Freestream velocity	40–65 m/s
Ramp angle of attack	0–10 deg
Microjet control parameters	
Diameter	400 μm
Location	Mj2–Mj7
Angle w.r.t. surface	68–105 deg
Pressure	0–25 psig
Separated flowfield parameters for PTC (5 deg, 40 m/s, $Re = 1.3e6$)	
Separation begins	$X/H = 1.7 \pm 0.02$
Reattachment	$X/H = 2.9 \pm 0.02$
Boundary- layer parameters at leading edge ($U_\infty = 40$ m/s, $Re = 1.3e6$)	
δ	18 mm
δ^*	3 mm
θ	2 mm

III. Results and Discussion

A. Velocity Field

1. *Baseline Case: No Control*

Velocity field data were obtained using 2-D PIV along the centerline plane. A representative of the ensemble averaged velocity field for the PTC is shown in Fig. 2, in which the ramp is at an angle of 5 deg (see Fig. 1b) and flow is from left to right. In these plots, the length scales are nondimensionalized by the ramp height, H. (Note that increasing the ramp angle of attack corresponds to increasing the adverse pressure gradient on the ramp surface). A closer look at Fig. 2a reveals that, as one proceeds downstream in the vicinity of the surface, there is a rapid deceleration in the fluid velocity, which eventually leads to a region of reverse flow. This reverse flow zone, which corresponds to dark blue velocity contours, starts at around $X/H = 1.7$ and extends to 2.9 ($H = 57.2$ mm), indicating that flow has separated locally, and a separation bubble with recirculating flow is clearly present. Velocity vectors for a small subsection confirming the presence of this reverse flow zone are shown as an inset in Fig. 2a. The contour corresponding to the reverse velocities is also shown as dotted lines in Fig. 2 to more clearly illustrate the size of the separation zone. In physical dimensions, the separation region for this case is ~68.6 mm (2.7 in.), which is considerably larger than cases in which the ramp is at lower angles; for example, for the 0 deg case, the recirculation bubble is only ~48.3 mm (1.9 in.) [28]. This of course is expected, because higher ramp angles result in more pronounced adverse pressure gradients and, hence, larger separation regions.

Similarly, increasing the freestream velocity increases the strength of the separation, that is, the magnitude of the reverse velocity in the flow, while the extent of separation region, which is due to the adverse pressure gradient, remains the same. To illustrate this, in Fig. 2c we show similar streamwise velocity field measurements for a freestream velocity of 65 m/s at an angle of attack of 5 deg. The maximum reverse velocity is increased by ~75% for the 65 m/s case as compared with the 40 m/s PTC case. Similar trends are observed in the vertical component of the velocity where low-velocity fluid is seen moving away from the boundary in the same region where reverse flowfield is seen in the streamwise velocity plots.

To summarize, the adverse pressure gradient generated due to the ramp geometry leads to local separation of the incoming boundary layer. The severity of separation in terms of the size of the separation region and the reverse velocity increases with the ramp angle due to an increasing adverse pressure gradient. An increase in the freestream velocity, on the other hand, increases the severity of

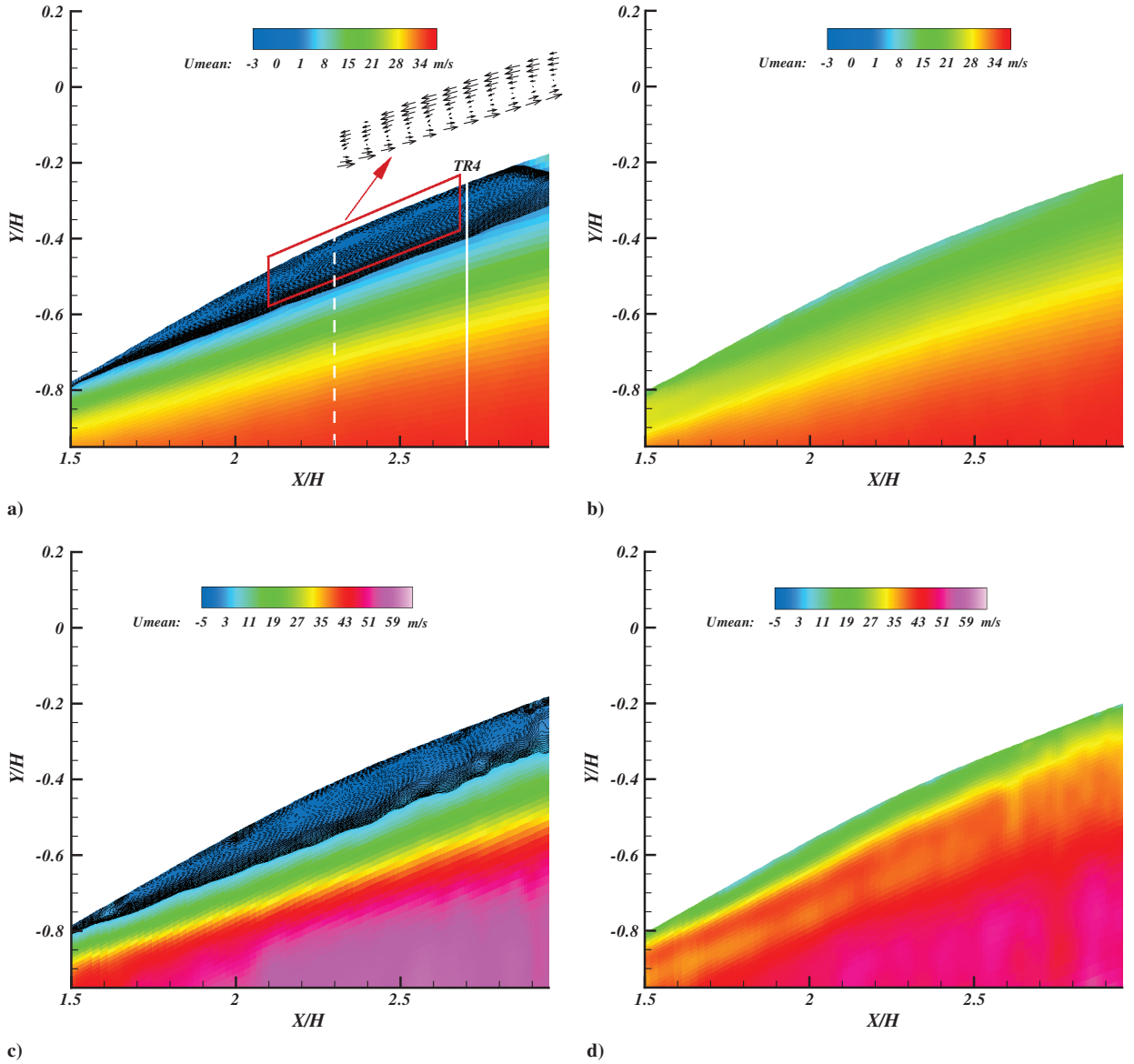

Fig. 2 Streamwise velocity data at a 5 deg ramp angle: a) 40 m/s: no control; b) 40 m/s: Mj4, 90 deg, 10 psig; c) 65 m/s: no control; d) 65 m/s: Mj5, 90 deg, 25 psig. The solid white line indicates the location of TR4, whereas the dashed white line indicates the location where velocity profile was extracted for Figs. 3b, 4, 8, and 11a.

separation by increasing the magnitude of reverse velocities. The presence of this separated flow is clearly evident in the measured velocity field. Hence, by varying either parameter, we can examine the effect of control on separation of varying sizes and strengths. In Sec. III.A.2, we examine the effect of microjet control on this separated flow.

2. Effect of Microjet Control

When microjets were activated at suitable locations, it was observed that the reverse or separated flow region was completely eliminated, with very low mass flux. This may be verified by the velocity contour plot shown in Fig. 2b, in which the microjet array, Mj4, which is at an angle of 90 deg relative to the local surface, has been activated at a stagnation pressure of 10 psig. This effect of microjets was observed for all the conditions examined, that is, wherever separated flow was present for the baseline case, microjets completely eliminated separation when activated at appropriate conditions. This is evident in Fig. 2d, in which the much stronger separated flowfield corresponding to a freestream velocity of 65 m/s is eliminated by activating Mj5 at 25 psig. A comparison of the control cases with the corresponding baseline cases (Figs. 2a and 2c) indicates that the activation of microjets not only eliminates the reverse flow but also increases the momentum near the surface significantly. This effect of microjet control and the optimization procedure, that is, identifying parameters to formulate a control strategy that has a maximal impact with minimal effort, is discussed later in Sec. III.C.

In addition to simply characterizing the effect of separation and its control on the unsteady surface flow, another aim of this study was to identify surface properties that are sensitive to the state of the flow away from the surface. These can in turn be used as "sensors" or inputs for a control strategy. A comparison of the fluctuating velocity field components, such as V_{rms} and U_{rms} (not shown here), clearly shows that separation is characterized by a significant increase in the flow unsteadiness. In addition, microjet control, which reattaches the flow, leads to dramatic reductions in these fluctuating velocities. Hence, it is reasonable to hypothesize that the unsteady surface pressure field and its response to actuation will display similar trends. Although P_{rms} cannot provide us with the detailed knowledge of the state of the flow; it might be possible to obtain an approximate representation of certain flow characteristics such as location and severity of separation. Consequently, as discussed next in Sec. III.B, we examined the unsteady surface pressures as a means of identifying the state of the separated flowfield.

B. Unsteady Pressures

High-frequency-response Endevco® (Model 8510B-1) pressure transducers with a range of 0–1 psi were used to measure the unsteady pressures at selected locations. These sensors were placed so that they were located both upstream of and within the separated region. The location of these transducers was discussed in Sec. II.A and is shown in Fig. 1 as TR1–TR4. Representative dynamic pressure spectra from one of the transducers (TR4) located inside the separation bubble ($X/H = 2.7$) are presented in Fig. 3. The location of this transducer with respect to the flowfield has also been indicated in Figs. 2a and 2c as a solid white vertical line. Measurements shown in Fig. 3 include the spectra for flow with and without control for the 0 and 5 deg angle of attack cases.

1. Baseline Case: No Control

A comparison of the spectra shown as solid lines in Fig. 3a shows that, for the baseline flow, the pressure fluctuations increase dramatically as we increase the ramp angle from 0 to 5 deg. The shift in spectra between the 0 and 5 deg cases shown in this plot represents a significant increase, by almost a factor of 2, in the overall P_{rms} levels. This behavior is also reflected in the corresponding velocity profiles shown in Fig. 3b, obtained at $X/H = 2.3$, in the middle of separation bubble indicated as a dashed vertical white line in Fig. 2. It can be noticed from Fig. 3b that an increase in the angle of attack increases the magnitude of the mean reverse velocity and the size of the separation bubble (seen as an increase in the vertical distance for which the reverse velocity is observed). This is also accompanied by a substantial increase in the velocity fluctuations, V_{rms}, in the separated region as the separation size becomes increasingly large. The correlation between the velocity field above the surface and the unsteady pressures suggests that the unsteady pressure distribution may be used as a measure of the separation location and its strength. This issue is explored in more detail in Sec. III.C.

2. Effect of Microjet Control

The unsteady pressures and the mean streamwise velocity with the microjets activated are also presented in Figs. 3a and 3b, respectively, as dashed lines. For the cases shown here, the microjets are operated at a stagnation pressure of 10 psig at an angle of 90 deg relative to the local surface. It is evident that the activation of microjets results in complete flow attachment (Fig. 3b) and a concomitant, significant reduction in the magnitude of the pressure fluctuations (Fig. 3a) for both the 0 and 5 deg cases. For the 5 deg case shown here, the pressure

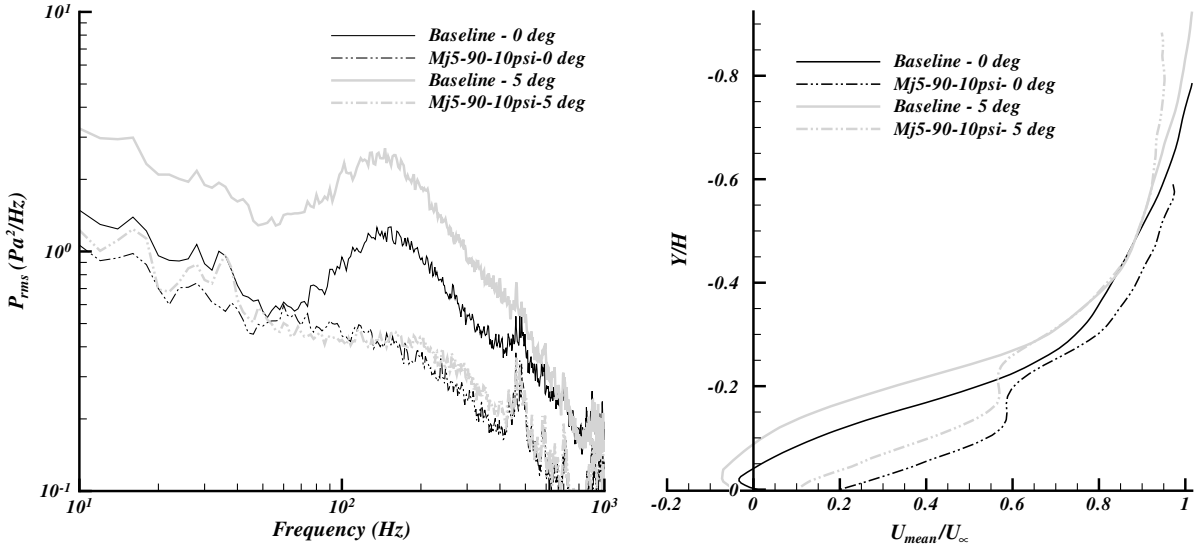

a) b)

Fig. 3 Response with and without control: a) unsteady surface pressure, $X/H = 2.7$, $U_\infty = 40$ m/s; and b) mean streamwise velocity profile, $X/H = 2.3$, $U_\infty = 40$ m/s.

fluctuations have been reduced by almost a factor of 2. This clearly illustrates the beneficial effects of the present flow control strategy, while again pointing to the use of unsteady surface pressures as a possible sensor for closed-loop/adaptive control strategies.

To summarize, microjets were very effective in controlling separation and attaching the flowfield globally. This phenomenon is also reflected in unsteady pressure distribution over the surface. How sensitive the unsteady pressure (distribution) is to microjet control and the state of the flowfield is critical to its potential use as a measure of the flow state. This is explored through a systematic, parametric study of microjet parameters on the flow properties, specifically the velocity and the unsteady pressure field, presented in Sec. III.C.

C. Efficacy of Microjet Control: Parametric Study

1. Microjet Location

The location of actuation with respect to separation location has been found to be a critical parameter by numerous investigators [10,25,33]. It stands to reason and is generally believed that actuation closer to the separation location would produce the most beneficial results. Using our velocity field measurements, the separation location for the given flow conditions was known. Accordingly, the flowfield was examined for a number of cases in which the microjet actuators were placed at varying distances, both upstream and downstream, relative to the separation location. As discussed subsequently, the velocity field data reveal that, in general, the microjets are most effective when activated upstream and close to the separation location. There appears to be a range of locations upstream of and close to separation where their effect is near optimal; once outside this range, that is, too far upstream, the effect of control diminishes. Similarly, locating the actuators downstream of the separation is also nonoptimal. However, for *all the actuator locations* examined to date, separation control could be achieved when the microjets were operated at a sufficiently high pressure. The difference is that the required pressure and, hence, the required mass flow increase if the actuators are outside the optimal region, that is, too far upstream or downstream of separation.

To facilitate our discussion, Table 1 provides the approximate locations for the separation, actuators, and the unsteady pressure transducers. A representative example of the velocity profiles for the 40 m/s case at a ramp angle of 5 deg is presented in Fig. 4, in which U/U_∞ is shown as a function of the vertical distance from the surface (Y/H) at a streamwise location of $X/H = 2.3$. As in Fig. 3b, the location at which these data were extracted from the velocity field is shown as a dashed vertical white line in Fig. 2 and roughly corresponds to the maximum reverse velocity in the separated region. For the controlled cases, the microjet angle relative to the surface is 68 deg and the microjet stagnation pressure is 10 psig. As evident in Fig. 4a, microjets at different locations have a measurably different effect on the velocity profile. Keeping in mind that for this case flow separates roughly at $X/H \sim 1.7$, the activation of Mj2, which is significantly upstream (at $X/H \sim 0.7$), at 10 psig does not lead to complete attachment and very small reverse velocities can still be seen in the plot. In contrast, flow is completely attached and the velocity profiles become much fuller with the activation of Mj5, which is located at $X/H \sim 1.3$, that is, much closer to, but still upstream of, separation. Along the same lines, when Mj7, located just downstream of the separation location at $X/H \sim 1.9$, is activated, the velocity profile deteriorates slightly relative to Mj5, although the difference is minimal. In addition to a reduction in the overall fluctuations, that is, the P_{rms} levels, changes in the spectral content can also be observed due to control. For example, in Fig. 5a, the use of Mj2 shifts the broad peak in the baseline flow to higher frequencies while also attenuating its amplitude. It is reasonable to assume that the spectral features are at least in part related to the length and time (or velocity) scales associated with the flowfield [34]. Hence, a shift to higher frequency may in part reflect the fact that the overall scale or size of the separation region has been reduced, as is indeed the case here. These aspects of the unsteady pressure behavior are being examined in an attempt to gain further insight into the flowfield's response to control [29]. In this paper, we are mainly

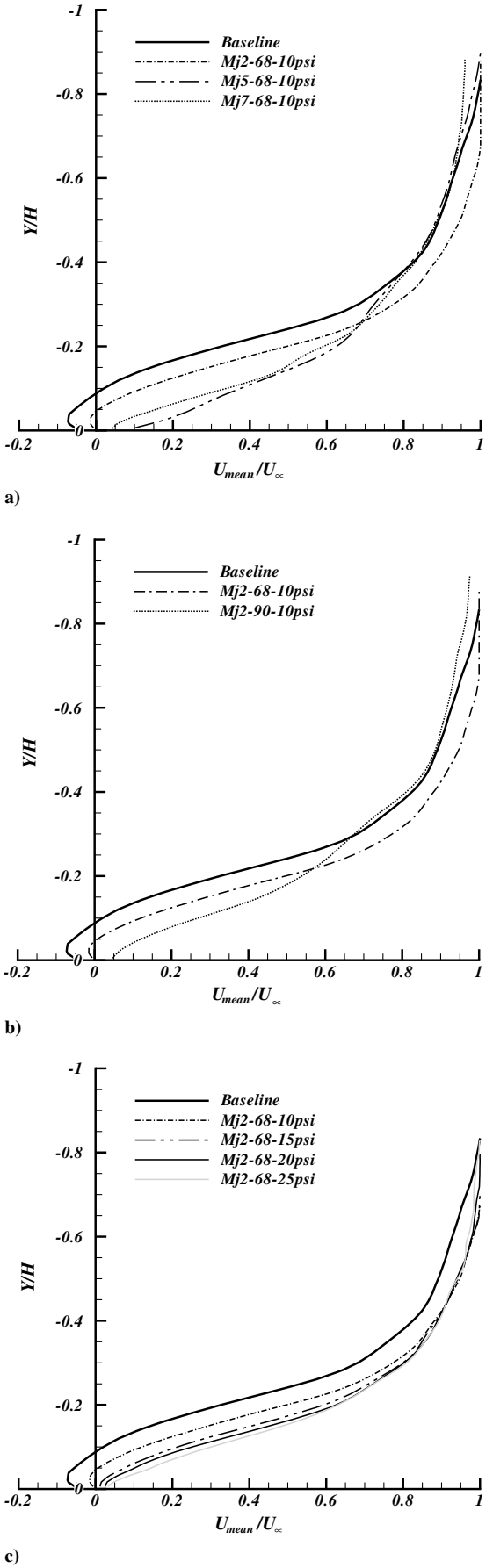

Fig. 4 Effect of parametric variation on the mean streamwise velocity profile, $X/H = 2.3$, $U_\infty = 40$ m/s, ramp angle = 5 deg: a) Mj2, Mj5, and Mj7: 68 deg; 10 psig; b) Mj2: 68 deg, 90 deg; 10 psig; and c) Mj2: 68 deg; 10, 15, 20, and 25 psig.

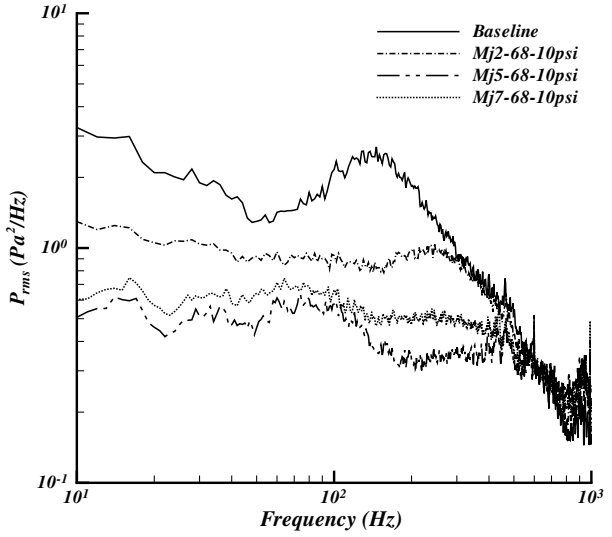

Fig. 5 Effect of parametric variation on the unsteady pressure spectra, $X/H = 2.7$, $U_\infty = 40$ m/s, ramp angle = 5 deg (Figs. 5a–5c correspond to the velocity profile in Figs. 4a–4c): a) Mj2, Mj5, Mj7: 68 deg; 10 psig; b) Mj2: 68 deg, 90 deg; 10 psig; and c) Mj2: 68 deg; 10, 15, 20, and 25 psig.

using the overall energy levels, P_{rms}, to examine the effect of control on the global properties which, as subsequently discussed, are very useful in developing practical control schemes.

The corresponding unsteady pressure distribution at $X/H = 2.7$, shown in Fig. 5a, reveals trends that are very similar to the velocity field with higher overall P_{rms} values for Mj2 where the flow is only partially reattached. As was the case for the mean velocity profiles of Fig. 4a, the P_{rms} distributions of Mj5 and Mj7 are very similar, primarily because the flow is completely attached for both cases. Partial flow attachment for Mj2 at these conditions, however, does not imply that the flow can not be attached. For example, using Mj2, separation could be completely eliminated using either a different microjet angle or a higher pressure. To illustrate this, a representative result, using Mj2 but with a different microjet angle, is shown in Fig. 4b. Here the microjet angle relative to the ramp surface is 90 deg. It is evident that, by using the same microjet pressure (10 psig), the flow is now *completely attached* where the Mj2 array is activated. Although not discussed in this paper, our results show that when 90 deg microjets are used, flow attachment is achieved at all actuator locations examined, that is, Mj2–Mj7. Similar effects are observed in the corresponding unsteady pressure measurements shown in Fig. 5b, in which the spectra for Mj2 at two different injection angles are compared. As seen in the plot, there is a significant reduction in the overall P_{rms} values at 90 deg relative to 68 deg. Given that the flow is still partially separated for 68 deg and attached for 90 deg, these results further substantiate the fact that P_{rms} is a good indicator of the flow state in terms of the degree to which it is attached or separated.

The same effect, although not as dramatic, can also be observed by increasing the microjet pressure. This is shown in Fig. 4c, in which the microjet pressure is varied while keeping the microjet angle (68 deg) and location (Mj2) fixed. The flow is completely attached at a pressure of 15 psig, and the velocity profile continues to become fuller as the microjet pressure is further increased. The unsteady pressure distribution for this case is shown in Fig. 5c. Similar observations can be made in that, as the microjet stagnation pressure is increased, the pressure spectra show a reduction in P_{rms}. However, it is important to note that, once flow is attached, Figs. 4c and 5c also indicate that successive increments in the microjet pressures yield increasingly lower returns in terms of additional momentum in the boundary layer, that is, fuller profiles, and lower P_{rms} values. This issue is further addressed in Sec. III.C.3.

The P_{rms} values or range of values that indicate complete attachment has yet to be explored and is addressed later in this paper. Nevertheless, the results discussed so far suggest that, with proper scaling, this property may be used to approximately identify the state of the flow, at least in the context of separation control. This effect on P_{rms} is investigated further to quantify the effect of microjet location on the flowfield and is presented next.

To examine the effect of microjet location with respect to separation independently, we fixed the microjet angle at 90 deg and examined the effect of microjet location for various pressures. In addition, to ensure that the data do not reflect any direct effect of the microjets on the transducer signal, we fixed the microjet location (X_{Mj}) with respect to transducer (X_T) and changed the separation location (X_s) by changing the angle of attack of the incoming flow. Thus, a change in P_{rms} should be influenced only by the actuator placement (X_{Mj}) with respect to separation location (X_s), that is, $X_s - X_{\text{Mj}} = \Delta X_{\text{Mj},S}$. To illustrate this effect, we show the reduction in unsteady pressures normalized by the baseline unsteady pressure, from hereon referred to as $\mathbf{\Psi_P}(=\Delta P_{\text{rms}}/P_{\text{rms,baseline}})$, as a function of $\Delta X_{\text{Mj},S}$. This has been shown in Fig. 6a, in which unsteady pressure measurements using TR4 have been used for five different separation locations (adverse pressure gradient) and, hence, five different $\Delta X_{\text{Mj},S}$. The inset in Fig. 6a also illustrates the test case, in which X_T and X_{Mj} (and, hence, $\Delta X_{\text{Mj},T}$) are held constant and only X_s is varied. The separation location for these cases was obtained using 2-D PIV measurements and has been nondimensionalized with microjet diameter (d_{Mj}). As can be seen in Fig. 6a, the reduction in P_{rms} values for various $\Delta X_{\text{Mj},S}$ shows a distinct trend with increasing C_μ [28]. Here, C_μ or the steady momentum coefficient is the nondimensionalization

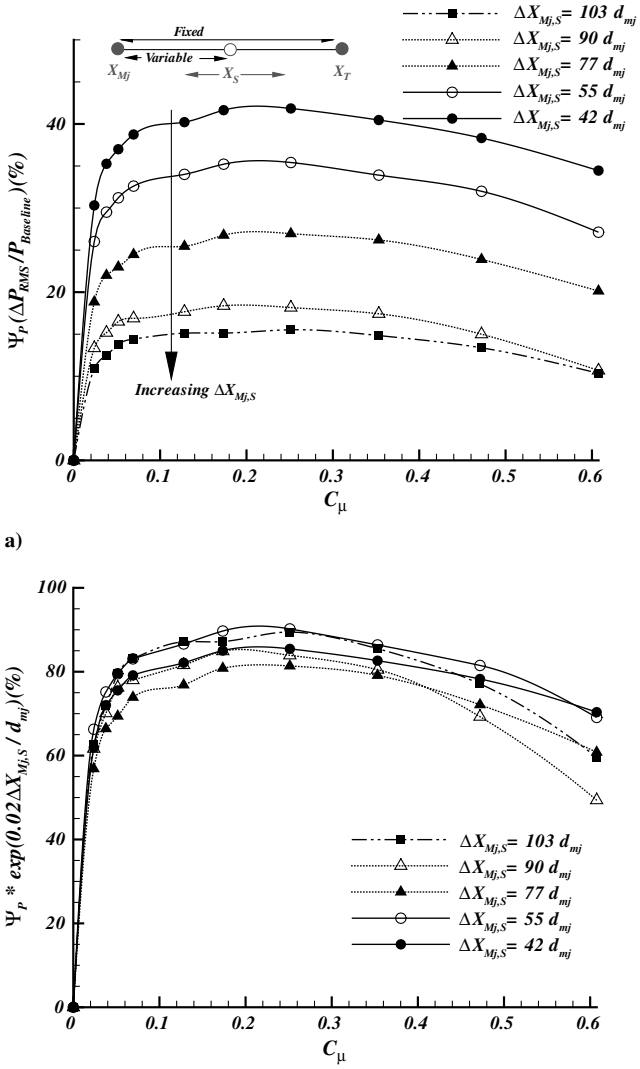

Fig. 6 $P_{\rm rms}$ reduction: a) effect of microjet location with regard to separation, and b) nondimensionalized effect of location.

parameter for the microjet pressure and is defined as the ratio of magnitude of total momentum injected into the flow relative to the freestream dynamic pressure multiplied with an appropriate area, chosen as δw in this case, that is,

$$C_\mu = \frac{Nm_{in}U_j}{\frac{1}{2}\rho_\infty U_\infty^2 \delta w} \tag{1}$$

where N is the number of microjets, m_{in} is the mass flow through a microjet, U is the jet velocity, ρ_∞ is the freestream density, U_∞ is the freestream velocity, w is the width of the model, and δ is the boundary-layer thickness at the ramp leading edge [28]. Boundary-layer thickness is often used in describing the inlet flow conditions for inlets/diffusers ingesting thick boundary layers such as BWB [35]. This is why we use the boundary-layer thickness instead of the momentum or displacement thickness in this definition. Use of C_μ for varying microjet pressures is discussed further in Sec. III.C.3.

Two distinct trends are seen here. First, the reduction in the unsteady pressures initially increases rapidly with increasing C_μ and then saturates. This is observed for all five cases in Fig. 6a, further reinforcing the fact that $P_{\rm rms}$ (or a reduction in $P_{\rm rms}$) is a very good indicator of the control effectiveness. Secondly, as seen in Fig. 6a, as the microjet is moved further away from the separation location, that is, increasing $\Delta X_{{\rm Mj},S}$, the effect in terms of $P_{\rm rms}$ reduction (Ψ_P) decreases. The decrease in gains with increasing $\Delta X_{{\rm Mj},S}$ is roughly exponential and can be nondimensionalized with $\exp(-(X_S - X_{\rm Mj})/(d_{\rm Mj}))$. The effect of nondimensionalization is shown in Fig. 6b. Thus, the scaling factor for microjet location $\Psi_P(L)$ has the functional form

$$\Psi_P(L) = \frac{1}{\exp\{[K_L(X_S - X_{Mj})]/d_{\rm Mj}\}} \tag{2}$$

where K_L is an empirical constant ($K_L = 0.02$ for the present case).

It should be noted here that the microjet may or may not have a direct effect on the transducer. Our test conditions do not provide us with a sufficient range of data to explore this effect conclusively. However, in the aforementioned case, the direct effect of the microjet on the transducer was kept constant; as such, the expression reflects the relative behavior of microjet location with respect to the separation. Figure 6b also indicates that, with increasing microjet pressure, there is an exponential saturation effect on $P_{\rm rms}$ reduction. This is because, once the flow is attached, additional momentum produces no benefit. This effect of pressure for an arbitrary location is further discussed in Sec. III.C.3. In summary, placing the microjet very close and upstream of the separation is ideal.

Having established that the worst control case scenario (farthest upstream of the separation location) also attaches the flowfield completely, if sufficient supply pressure/microjet momentum is used, and that the unsteady pressure reflects these characteristics, we now move on to other control parameters. The results discussed earlier naturally suggest two additional parameters of importance, namely, microjet angle and microjet pressure, which appear to have a significant impact on the flow properties and the control efficacy.

2. *Microjet Angle*

The microjet angle here refers to the *angle relative to the local surface* through which flow is injected into the main flow stream. Four different angles ranging from 68 to 105 deg with regard to the local surface were examined. These angles represent the minimum and maximum injection angles within the constraints of our present setup. It should be mentioned here that 68 deg does not mean that the microjets are blowing opposite to the freestream. For example, for Mj5, after taking ramp geometry and ramp angle into account, it is blowing at an angle of 3 deg with respect to and in the direction of the freestream. For ease of understanding, the microjet injection angles with respect to the ramp surface and the freestream are shown in Fig. 7.

The effect of microjet angle control was primarily examined at two locations, Mj4 and Mj5, mainly to understand whether the effects of the microjet angle and location are coupled and if there is an optimal angle for microjet control. Representative velocity profiles at $X/H = 2.3$, with microjets activated at Mj4 and Mj5, are shown in Fig. 8. Similar to those shown in Fig. 4, these profiles were extracted from whole field velocity (PIV) data and the microjets are operated at a constant pressure of 10 psig for all the cases shown in Fig. 8.

In Fig. 8a, velocity profiles where the microjet array Mj4 has been activated are shown. Using the fullness of the profile as a qualitative

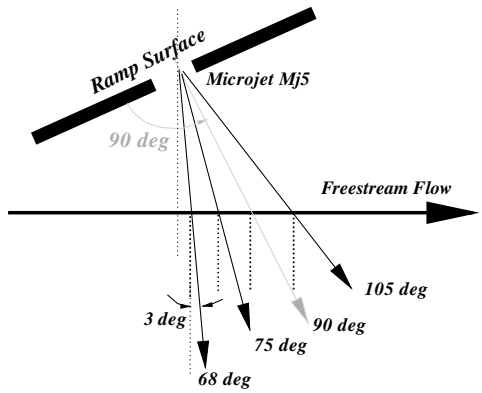

Fig. 7 Microjet angles with respect to the local surface and freestream for Mj5.

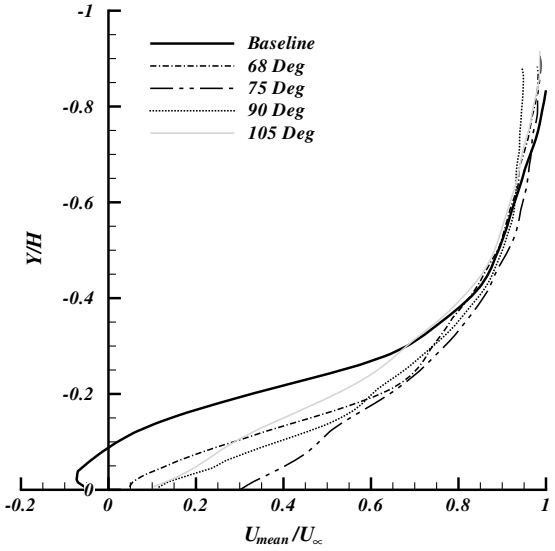

a)

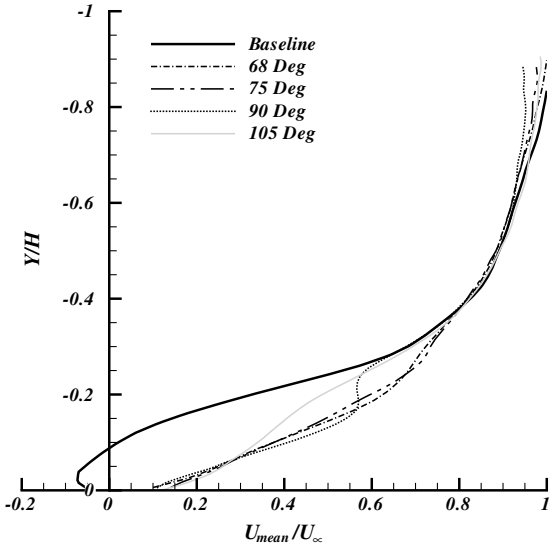

b)

Fig. 8 Effect of parametric variation (angle) on the mean streamwise velocity profile, $X/H = 2.3$, $U_\infty = 40$ m/s, ramp angle = 5 deg: a) Mj4: 68, 75, 90, and 105 deg; 10 psig; and b) Mj5: 68, 75, 90, and 105 deg; 10 psig.

measure, that is, the presence of high-momentum fluid near the surface, these velocity profiles suggest that optimal control is achieved with an injection angle of 75 deg. It is also evident that the 68 deg injection angle produces a profile that is not as full as the 90 deg case. This suggests that there is an optimum angle to achieve the best results.

To verify whether this optimum angle is coupled with location, similar experiments were performed with the array Mj5. These results are shown for $X/H = 2.3$ in Fig. 8b. It can be seen that the optimal angle is no longer 75 deg. In fact, there is very little difference in the profiles in the near-wall region, between the 68, 75, and 90 deg injection angles. This is indicative of the complex flow behavior and the strong interdependence between the various control parameters. This also suggests the need for another metric, or metrics, that capture the effect of more than one parameter. Nevertheless, even though we are still working toward understanding the details of the various parametric effects to further fine tune and optimize the use of microjets for separation control, what is encouraging is the fact that this very simple approach is relatively robust, in that it yields significant benefits over a wide range of conditions with very little cost.

The unsteady pressure distributions shown in Fig. 9 further confirm the trends observed in the corresponding velocity profiles shown in Fig. 8. In the case of Mj4 shown in Fig. 9a, the 75 and 105 deg injection angles seems to be performing better. However, the difference in the spectra and the overall values for these cases is not very significant. This is probably because the flow is attached for all the control cases. Similarly, as seen in Fig. 9b, 68 and 105 deg are seen to perform better than 75 deg. This further confirms that the optimal control angle depends on the control location.

The question that naturally arises is "Why is the behavior different for different angles?" A closer study of Fig. 8 suggests that, for a given pressure, increasing the injection angle initially makes the velocity profile fuller; however, subsequent increments in the injection angle yield lower gains in terms of added momentum in the near-wall region. This may be explained as follows. As the angle is increased, an increasingly larger percentage of the vertical component of momentum is being distributed to the horizontal component. Normally, one would expect that, as the horizontal component of the microjet fluid is increased, the profile would become increasingly fuller. However, an examination of the earlier results reveals that this is not the case. *Hence, direct momentum injection is not the principal*

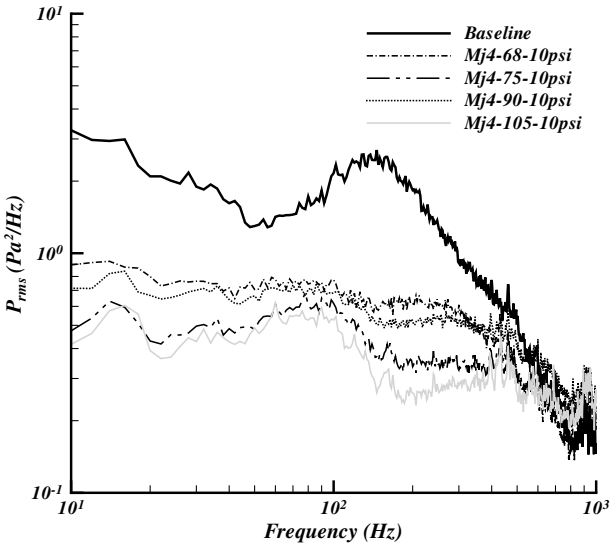

a)

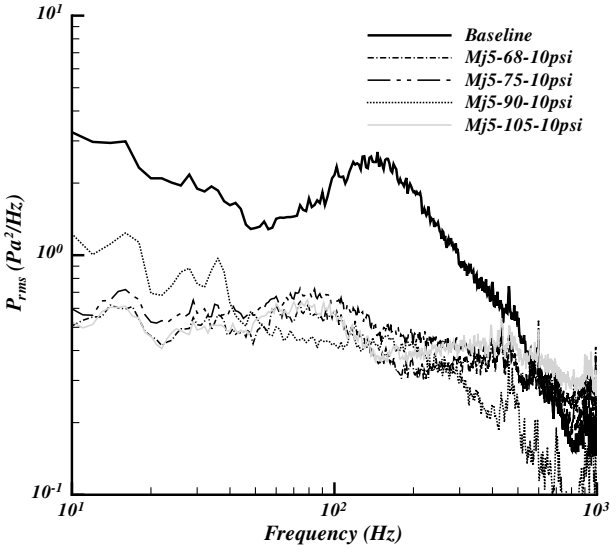

b)

Fig. 9 Effect of parametric variation (angle) on the unsteady pressure spectra, $X/H = 2.7$, $U_\infty = 40$ m/s, ramp angle = 5 deg: a) Mj4: 68, 75, 90, and 105 deg; 10 psig; and b) Mj5: 68, 75, 90, and 105 deg; 10 psig.

mechanism behind separation control in the present approach. If direct momentum injection was the primary mechanism, as has been the case with traditional wall tangential blowing [36], the mass flow rate required would be dramatically higher. In fact the momentum added once the flow is attached is at least an order of magnitude greater than the total momentum injected via the microjets (see Kumar and Alvi [28] for more details).

It is well known that jets in crossflow, which is in essence the flow generated by the actuation of microjets, can generate longitudinal or streamwise vortices [37–39] in a boundary layer. These vortices in turn appear to increase cross-stream mixing, thus increasing the streamwise momentum of the near-wall fluid. It was our expectation that, in a manner similar to (but perhaps more efficient than) physical vortex generators and air-jet vortex generators [37], high-speed microjets would energize the boundary-layer fluid by creating strong streamwise vorticity [38], thereby enhancing mixing with the more energetic flow. The strength of these streamwise vortices should be proportional to the strength of the jet in the crossflow, at least to a first order. As one increases the injection angle, the vertical momentum of the jet that characterizes the strength of the jet in crossflow is getting weaker. As such, the enhanced mixing effect due to the streamwise vortices is reduced; hence, lower gains are observed. Before further exploring efficiency as a function of injection angle, it is worth noting that the generation of streamwise vorticity by air jets or jets in crossflow is not a new mechanism [37–39]. However, given the very small size of the present microjets, their penetration depth is limited to a fraction of the boundary layer [28,29], which makes this approach somewhat different than the standard air jets used in most studies. This also makes them akin to sub-d-scale vortex generators, which are found to be more effective in controlling separation [12]. *This, combined with the very low mass flux needed, again due to the small size, makes them an efficient separation control device.*

In essence, the control efficiency due to microjet injection angle is a tradeoff between the direct addition of momentum and momentum gain via enhanced mixing due to the generation of the streamwise vortices. At lower angles of injection with regard to freestream, mixing is enhanced due to the streamwise vortices. As we increase the injection angle, directing a larger component of the microjet flow in the freestream direction, momentum is directly injected into the flow, but weakens the streamwise vortices. With the higher injection angle and, as such, a weaker jet in crossflow, the effect created by these streamwise vortices is reduced. This reduction due to secondary effects generated by the microjet is probably not compensated for by the redirection of momentum parallel to the surface. The effect of streamwise vorticity is currently being investigated in more detail using three-component PIV measurements. However, our results clearly indicate is that it is not just the direct addition of momentum; rather, it is the stronger secondary effect, created by the streamwise vortices, which is dominant in the present flow control approach. As such, in seeking the optimal injection angle, one may expect two peaks in the P_{rms} reduction or the momentum gain for a given flowfield and actuator. The magnitude of these peaks should be dependent on the microjet location with regard to separation.

To investigate this effect of microjet angle on momentum addition, as a first step, we examined the effect of Mj4, a fixed microjet location, with varying microjet pressures. The momentum gain ratio (MGR) is defined as the ratio of the increase in momentum due to microjets relative to the momentum injected by the microjets [28], that is,

$$\text{MGR} = \frac{\text{momentum}_{\text{With Control}} - \text{momentum}_{\text{No Control}}}{\text{momentum}_{\text{microjets}}} = \frac{\int(\rho U \mathrm{d}A)_{\text{With Control}} - \int(\rho U \mathrm{d}A)_{\text{No Control}}}{N\dot{m}_{in}U_j} \tag{3}$$

A comparison of MGR for different microjet angles at various C_μ is plotted in Fig. 10a. As clearly seen here, upon increasing the microjet angle from 68 to 75 deg, we observe an increase in MGR for all operating pressures. A further increase in microjet angle from 75 to 90 to 105 deg results in a decrease in MGR. However, this effect of microjet angle changes as we move closer to the separation location. This is shown in Fig. 10b, in which MGR for both Mj4 and Mj5 has been plotted for a constant microjet pressure of 10 psig. Although these data suggest that the peaks and valleys in the variation with angle might exist, the presence of two optimal angles cannot be conclusively demonstrated due to the limited range of available data. A more comprehensive investigation that includes additional microjet angles and other microjet parameters and has a lower sensitivity to actuator input needs to be conducted to better understand the effect of microjet angle.

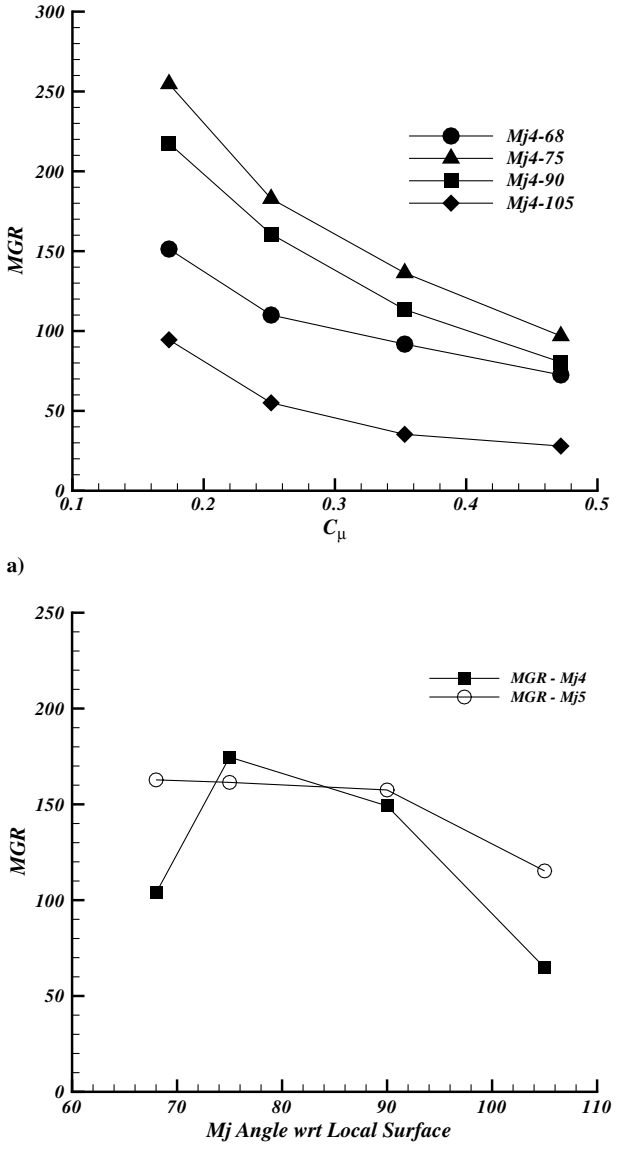

Fig. 10 Effect of microjet angle: a) MGR, $X/H = 2.3$, $U_\infty = 40$ m/s, ramp angle = 5 deg; and b) optimal angle variation with location, $U_\infty = 40$ m/s, ramp angle = 5 deg, microjet pressure = 10 psi.

Nevertheless, it can be safely concluded that the effect of microjet angle is coupled with microjet location. To determine the optimal angle, the optimal location needs to be identified first. With this in mind and recognizing that the effect of microjet angle is negligible on Mj5 (see Fig. 10b) for the present cases, we next examine the effect of microjet pressure on the flowfield.

3. *Effect of Microjet Pressure*

As mentioned earlier and evident from the results presented thus far, microjet pressure is also a significant control parameter. As seen

in Figs. 4 and 5, at certain locations, a higher microjet pressure is required to eliminate separation. To further explore this, we varied the microjet pressure at the "optimized control location," that is, the location that required the least amount of momentum influx for control. This corresponds to Mj5, where we also fix the injection angle to 90 deg. Representative velocity profiles of the streamwise component from this experiment are shown in Fig. 11a for $X/H=$ 2.3. As seen from Fig. 11a, the separation was well controlled at 2 psig and saturation was observed beyond 7 psig. This variation in the control effect was also seen in the unsteady pressure measurements shown in Fig. 11b. The spectra shown in Fig. 11b reveal that overall P_{rms} values decrease as the microjet pressure is increased, but that, after 10 psig, the microjet effect is saturated. In fact, with increasing microjet pressure, beyond 20 psig, the P_{rms} values begin to slightly increase. This can be seen in Fig. 11b, in which the spectra for 25 and 30 psig, indicated as gray lines, are relatively higher than those for 10 psig. This effect is not observed in the mean velocity profiles. However, if one examines the velocity fluctuations, shown in Fig. 11c, it is seen that U_{rms} decreases with increasing microjet pressure up to 10 psig, becomes saturated, and then increases for 25 and 30 psig. This is expected because, once the flow is attached, any additional disturbance will lead to higher fluctuations. This effect of microjet location has already been discussed earlier in Sec. III.C.1. It also indicates that there exists an optimal operating pressure range (for a given microjet location and orientation) and that, outside this, the microjets may increase the unsteadiness in the flow. However, the increase in noise is much lower than the reduction due to flow reattachment.

The next question that is raised is "What should be the criterion for control?" or "When have we achieved separation control for which further increases in the microjet pressure are not beneficial?" Should the criterion just be that the flow is incipiently attached everywhere or should further increments in momentum in the near-wall region of the boundary layer, that is, the fullness of the boundary-layer profile, and the unsteadiness associated in the flow also be considered? The answer to this question will likely come from a detailed cost function analysis, which is beyond the scope of this paper.

However, as an initial step, to gain some insight into the "costs" and benefits of this control approach, we plot the reduction in P_{rms} values (Ψ_P) for various microjet pressures at a 0 deg angle at 40 m/s and at a 5 deg angle at 65 m/s. The plot corresponding to these two cases, which represent the limits of our test parameter range, is shown in Fig. 12a. Two interesting points can be noticed:

1) There is an increase in the P_{rms} reduction (Ψ_P) up to 7 psig for the 0 deg case, and a further increase in microjet pressure leads to a saturation effect, followed by an increase in P_{rms}. This was also observed and commented on earlier in Sec. III.C.1. This behavior is expected because, until the flow is fully attached and "stable," an increase in microjet pressure would provide additional mixing of low-momentum boundary-layer fluid with the high-momentum fluid. Once it reaches saturation, additional momentum acts as a disturbance in the flow, thus increasing P_{rms}. These two opposing effects of microjet pressure again indicate the existence of an optimal pressure range.

2) The microjet pressure at which the P_{rms} reduction (Ψ_P) saturates, that is, no additional benefits are gained, varies with the angle of attack. This is anticipated, because the strength of separation varies with the angle of attack or the adverse pressure gradient and, as such, the pressure required to attach the flow is different. To take into account the incoming flow conditions, we have used non-dimensionalized pressure parameter C_μ (defined in Sec. III.C.1). Figure 12b shows the plot for the control of these two extreme cases with C_μ. As anticipated, the two P_{rms} reduction curves become similar and saturation can be observed at a $C_\mu \sim 0.17$. This non-dimensionalization of microjet pressure may allow our results to be extended to models and flows for other scales and applications. The resulting saturated curve, shown in Fig. 11b, has the following functional form:

$$\Psi_P(P) = 1 - K_{P1}^{\sqrt{C_\mu}}(\sqrt{C_\mu}+1)^{K_{P2}} \tag{4}$$

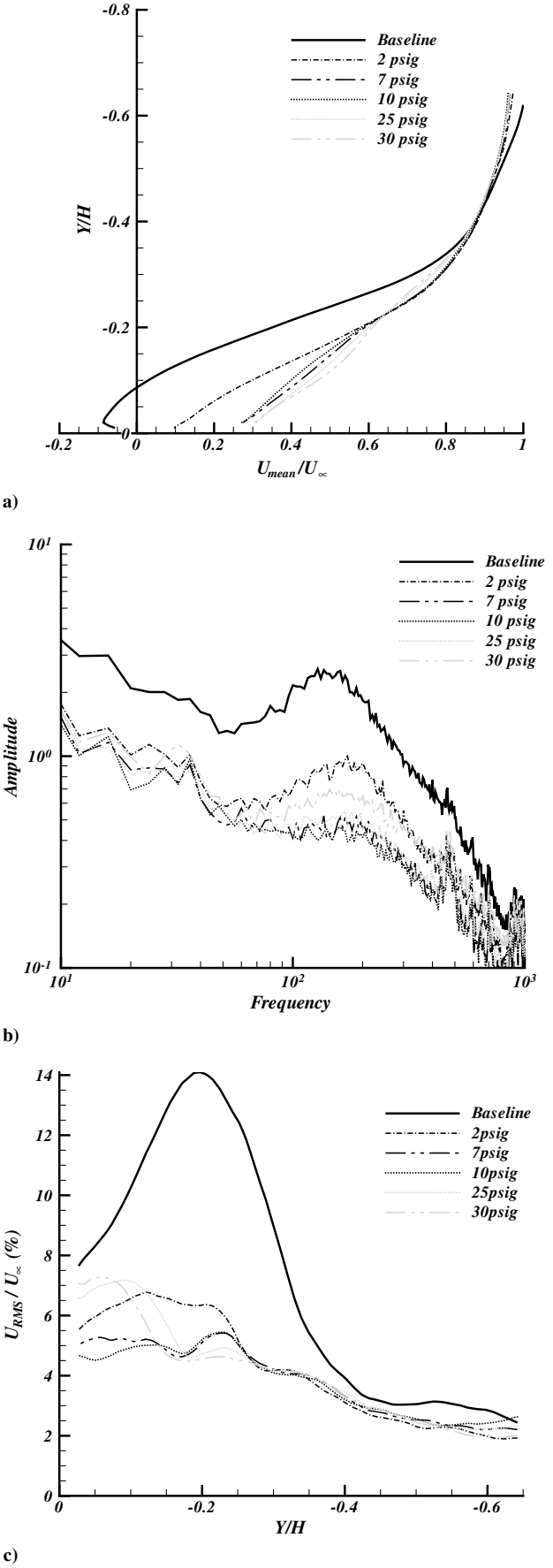

Fig. 11 Effect of microjet pressure: a) mean streamwise velocity profile, $X/H = 2.3$, $U_\infty = 40$ m/s, ramp angle = 5 deg; b) unsteady pressure spectra, $X/H = 2.7$, $U_\infty = 40$ m/s, ramp angle = 5 deg; and c) U_{rms}, $X/H = 2.7$, $U_\infty = 40$ m/s, ramp angle = 5 deg.

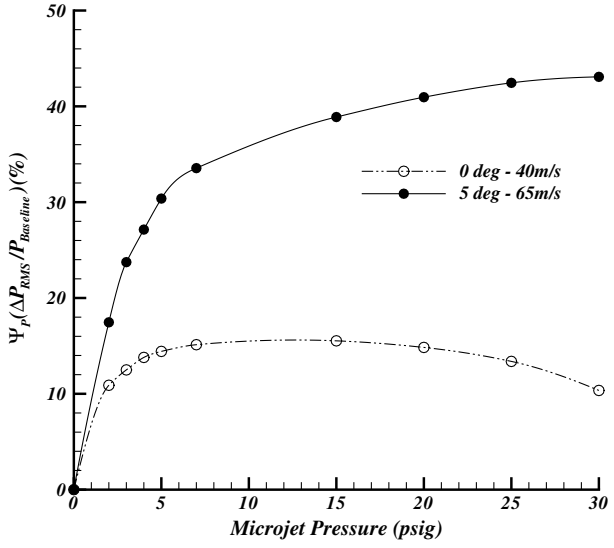

a)

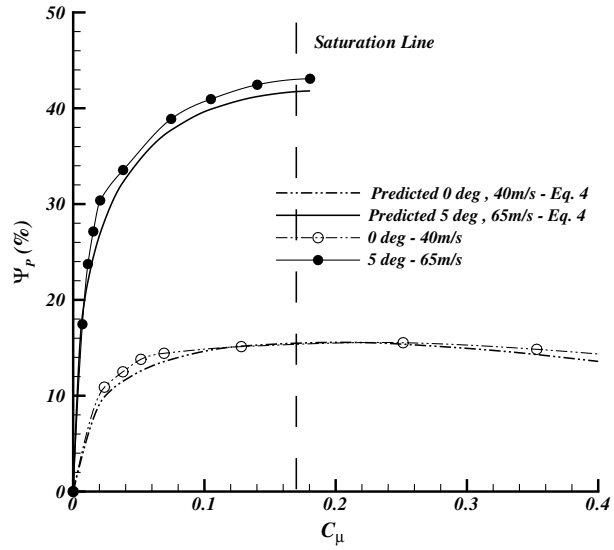

b)

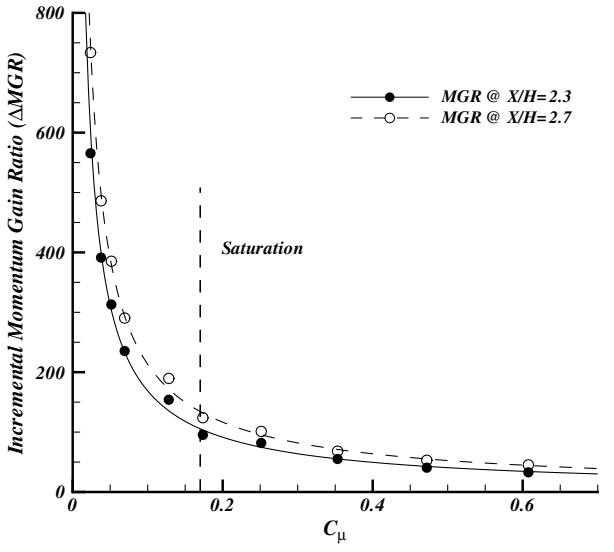

c)

Fig. 12 Effect of microjet pressure: a) P_{rms} reduction, $X/H = 2.7$, variation with microjet pressure for different incoming boundary layer; b) P_{rms} reduction, $X/H = 2.7$, microjet pressure nondimensionalized as C_μ; and c) MGR, $U_\infty = 40$ m/s, ramp angle = 5 deg.

where K_{P1} and K_{P2}, are constants that depend on the incoming flow conditions ($K_{P1} = 7.28$ and $K_{P2} = -2.9$ for the present 0 deg case).

The resulting curve from Eq. (4) is also shown in Fig. 12b as a solid line. Equation (4) can be considered to be representative of the two opposing effects of microjets, mentioned earlier. The pressure is modeled using C_μ to take into consideration its relative effect on the freestream conditions. The initial positive effect of the microjet on the separated flow is largely reflected in the positive power of C_μ as it saturates; further increments in the C_μ are reflected as a reduction in the beneficial effect of microjet pressure, indicating an optimal pressure or C_μ. As can be noticed from Fig. 12b, Eq. (4) captures the characteristics of the P_{rms} reduction with a variation in C_μ and can be used as scaling factor for microjet pressure (C_μ). The specific values of the parameters used in Eq. (4), for example, $C_\mu^{1/2}$, K_{P1}, and K_{P2}, were obtained using a best fit to the data over the entire range of conditions examined. This scaling needs to be further refined to take into account the incoming conditions to increase its generality. However, for a given geometry and flow conditions, the saturation effect can be easily deduced and, as such, it makes the present criteria for a selection of optimal pressure feasible in nature.

To verify if we have similar saturation effects on the momentum gain, we examined the incremental variation in MGR as a function of C_μ; this behavior is shown in Fig. 12c. When the flow is separated initially, very low microjet pressures yield high-momentum gains. Once the flow is attached, subsequent increments in the microjet pressure lead to relatively low incremental gains until it is almost saturated at 10 psig or $C_\mu = 0.17$. Because we observe the same behavior in saturation in terms of MGR as we do for P_{rms} reduction, it is reasonable to presume that the C_μ saturation value can be used as an indicator for optimal microjet pressure. It should also be noted that, unlike the P_{rms} reduction, MGR continues to increase, although minimally, with increasing C_μ beyond the "saturation" point. This is expected, because, by increasing the microjet pressure, we are increasing the momentum continually, albeit by very small increments. The most pertinent outcome is that *both* the P_{rms} reduction and MGR criteria indicate that the minimum cost with maximum effect added to the flow occurs when the saturation point is reached.

Based on the discussion until now, for a fixed microjet angle of 90 deg, the parameters that affect the reduction in unsteady pressure are the location of microjets with respect to separation ($\Delta X_{\text{Mj},S}$) and the microjet pressure or C_μ. In a functional form, this can be summarized as

$$\frac{\Delta P_{\text{rms}}}{P_{\text{rms,baseline}}} \quad \text{or} \quad \Psi_P = f(\Delta X_{\text{Mj},S}, C_\mu) = \Psi_p(L) \times \Psi_p(P) \tag{5}$$

Using the results from Eq. (1) (Sec.) and Eq. (4) (Sec.), we have a combined form as

$$\Psi_P = \frac{P_{\text{rms,baseline}} - P_{\text{rms,control}}}{P_{\text{rms,baseline}}} = \Psi_P(P) x \Psi_P(L)$$
$$= \frac{1 - K_{P1}^{\sqrt{C_\mu}}(\sqrt{C_\mu} + 1)^{K_{P2}}}{\exp(K_L(X_S - X_{\text{Mj}})/d_{\text{mj}})} \tag{6}$$

With known X_{Mj}, X_S, and C_μ, the P_{rms} reduction (Ψ_P) can be calculated and the optimal pressure can be determined based on the saturation point, which in our case is at $C_\mu = 0.17$ (10 psig).

With the use of optimized control parameters, one can significantly reduce the mass flow requirements. In our case, we reduced the required pressure by optimizing the microjet control parameters to fully control the flow with minimum unsteadiness from the earlier reported 25 to 10 psig. This reduction in pressure corresponds to a reduction in required mass flow by more than 40%. From a more practical perspective, for a pressure of 10 psig, when extrapolated to a theoretical inlet duct, for example, a 30% boundary-layer ingesting duct [35], a nominal value used for BWB inlet, this results in a mass flow requirement that is well below the maximum permissible bleed flow values as generally quoted by engine manufacturers. This

suggests that engine bleed flow may be used to supply the gas for the microjet actuators.

IV. Conclusions

To summarize, the results of this study, mainly based on velocity field and unsteady surface pressure measurements, clearly show the effect of microjets in effectively controlling flow separation over the entire range of conditions examined. More specifically, for the present geometry and range of flow conditions, the following conclusions can be drawn:

1) The effect of control varies with the amount of momentum supplied via the microjets (which is proportional to microjet *pressure*) and also with their *location* and the *angle* at which momentum is injected. These control parameters are coupled, yet by changing any variable to appropriate conditions, the separated flow can be attached.

2) In general, placing the microjets close to and upstream of the separation line, where control effectiveness decreases as one moves further away from separation, is optimal.

3) The unsteady pressure distribution is sensitive to the state of the flow and the effect of control on the flow. Although, the pressure may not be used to provide a complete description of the flow "state," it appears to be sufficient (at least in this geometry) to be used as sensor for determining the flow condition, that is, whether it is separated, the location, and an indication of the severity of the separation.

4) The response of the unsteady pressure to the flowfield P_{rms} (Ψ_P) reflects trends similar to the change in MGR. With appropriate scaling, correlations have been developed that may be implemented in closed-loop active control strategy, at least as a first step.

5) A better understanding of the effect of various flow and control parameters on the effectiveness of separation control can result in the development and refinement of scaling laws, similar to those presented here. Their implementation will in turn result in the development of optimal control strategies that produce the largest performance gains with minimal input.

We believe that, through the knowledge gained in this study, we are beginning to make progress toward our ultimate goal of using of these actuators in a closed-loop mode for optimal control. If properly used, together with appropriate sensors, these low-mass–high-momentum microjets show considerable promise for controlling flow separation.

Acknowledgments

This study has in part been supported by grants from the NASA Langley Research Center, grants that initiated this research, and from the Florida Center for Advanced Aero-Propulsion. We are grateful for this support.

References

[1] Anabtawi, A. J., Blackwelder, R. F., Lissaman, P. B. S., and Leibeck, R. H., "An Experimental Investigation of Boundary Layer Ingestion in a Diffusing *S*-Duct with and Without Passive Flow Control," AIAA Paper 99-0739, Jan. 1999.

[2] Mayer, D. W., Anderson, B. H., and Johnson, T. A., "3D Subsonic Diffuser Design and Analysis," AIAA Paper 98-3418, July 1998.

[3] Liebeck, R. H., "Design of the Blended Wing Body Subsonic Transport," *Journal of Aircraft*, Vol. 41, No. 1, 2004, pp. 10–25. doi:10.2514/1.9084

[4] Rabe, D., Boles, A., and Russler, P., "Influence of Inlet Distortion on Transonic Compressor Blade Loading," AIAA Paper 1995-2461, July 1995.

[5] Seifert, A., Darabi, A., and Wyganski, I., "Delay of Airfoil Stall by Periodic Excitation," *Journal of Aircraft*, Vol. 33, No. 4, 1996, pp. 691–698. doi:10.2514/3.47003

[6] Gad-el-Hak, M., and Bushnell, D. M., "Separation Control: A Review," *Journal of Fluids Engineering*, Vol. 113, No. 1, 1991, pp. 5–30. doi:10.1115/1.2926497

[7] Amitay, M., Pitt, D., and Glezer, A., "Separation Control in Duct Flows," *Journal of Aircraft*, Vol. 39, No. 4, 2002, pp. 616–620. doi:10.2514/2.2973

[8] Zaman, K. B. M. Q., Bar-Sever, A., and Mangalam, S. M., "Effect of Acoustic Excitation on the Flow over a Low-*Re* Airfoil," *Journal of Fluid Mechanics*, Vol. 182, 1987, pp. 127–148. doi:10.1017/S0022112087002271

[9] Ahuja, K. K., Whipkey, R. R., and Jones, G. S., "Control of Turbulent Boundary Layer Flows by Sound," AIAA Paper 1983-726, April 1983.

[10] David Greenblatt, and Wygnanski, I. J., "The Control of Flow Separation by Periodic Excitation," *Progress in Aerospace Sciences*, Vol. 36, No. 7, 2000, pp. 487–545. doi:10.1016/S0376-0421(00)00008-7

[11] Storms, B. L., and Ross, J. C., "Experimental Study of Lift-Enhancing Tabs on a Two-Element Airfoil," *Journal of Aircraft*, Vol. 32, No. 5, 1995, pp. 1072–1078. doi:10.2514/3.46838

[12] Lin, J. C., "Review of Research on Low-Profile Vortex Generators to Control Boundary-Layer Separation," *Progress in Aerospace Sciences*, Vol. 38, Nos. 4–5, 2002, pp. 389–420. doi:10.1016/S0376-0421(02)00010-6

[13] Sinha, S. K., "Flow Separation Control with Microflexural Wall Vibrations," *Journal of Aircraft*, Vol. 38, No. 3, 2001, pp. 496–503. doi:10.2514/2.2789

[14] Smith, B. L., and Swift, G. W., "A Comparison Between Synthetic Jets and Continuous Jets," *Experiments in Fluids*, Vol. 34, No. 4, 2003, pp. 467–472. doi: 10.1007/S00348-002-0577-6

[15] Santhanakrishnan, A., and Jacob, J. D., "Flow Control with Plasma Synthetic Jet Actuators," *Journal of Physics D: Applied Physics*, Vol. 40, No. 3, February 2007, pp. 637–651. doi:10.1088/0022-3727/40/3/S02

[16] Huang, J., Corke, T., and Thomas, F., "Plasma Actuators for Separation Control of Low-Pressure Turbine Blades," *AIAA Journal*, Vol. 44, No. 1, 2006, pp. 51–57. doi:10.2514/1.2903

[17] Moreau, E., "Airflow Control by Non-Thermal Plasma Actuators," *Journal of Physics D: Applied Physics*, Vol. 40, No. 3, 2007, pp. 605–636. doi:10.1088/0022-3727/40/3/S01

[18] Selby, G. V., Lin, J. C., and Howard, F. G., "Control of Low-Speed Turbulent Separated Flow Using Jet Vortex Generators," *Experiments in Fluids*, Vol. 12, No. 6, April 1992, pp. 394–400. doi:10.1007/BF00193886

[19] Peake, D. J., Henry, F. S., and Pearcey, H. H., "Viscous Flow Control with Air-Jet Vortex Generators ," AIAA Paper 1999-375, 1999.

[20] Krzysiak, A., "Control of Flow Separation Using Self-Supplying Air-Jet Vortex Generators," *AIAA Journal*, Vol. 46, 2008, pp. 2229–2234. doi:10.2514/1.30150

[21] Raju, R., Mittal, R., and Cattafesta, L., "Towards Physics Based Strategies for Separation Control over an Airfoil Using Synthetic Jets" AIAA Paper 2007-1421, Jan. 2007.

[22] Cannelle, F., and Amitay, M., "Synthetic Jets: Spatial Evolution and Transitory Behavior," AIAA Paper 2005-102, Jan. 2005.

[23] Glezer, A., Amitay, M., and Honohan, A. M., "Aspects of Low- and High-Frequency Actuation for Aerodynamic Flow Control," *AIAA Journal*, Vol. 43, No. 7, 2005, pp. 1501–1511. doi:10.2514/1.7411

[24] Glezer, A., and Amitay, M., "Synthetic Jets," *Annual Review of Fluid Mechanics*, Vol. 34, Jan. 2002, pp. 503–529. doi:10.1146/annurev.fluid.34.090501.094913

[25] Jenkins, L., Gorton, S. A., and Anders, S., "Flow Control Device Evaluation for an Internal Flow with Adverse Pressure Gradient," AIAA Paper 2002-0266, Jan. 2002.

[26] Zhuang, N., Alvi, F. S., Alkislar, M. B., and Shih, C., "Supersonic Cavity Flows and Their Control," *AIAA Journal*, Vol. 44, No. 9, 2006, pp. 2118–2128. doi:10.2514/1.14879

[27] Alvi, F. S., Shih, C., Elavarasan, R., Garg, G., and Krothapalli, A., "Control of Supersonic Impinging Jet Flows Using Supersonic Microjets," *AIAA Journal*, Vol. 41, No. 7, 2003, pp. 1347–1355. doi:10.2514/2.2080

[28] Kumar, V., and Alvi, F. S., "Use of High-Speed Microjets for Active Separation Control in Diffusers," *AIAA Journal*, Vol. 44, No. 2, 2006, pp. 273–281. doi:10.2514/1.8552

[29] Kumar, V., "Separation Control in Adverse Pressure Gradient Using High-Speed Microjets," Ph.D. Dissertation, Mechanical Engineering, Florida State Univ., Tallahassee, FL, 2008.

[30] Stratford, B. S., "The Prediction of Separation of Turbulent Boundary Layer," *Journal of Fluid Mechanics*, Vol. 5, Jan. 1959, pp. 1–16. doi:10.1017/S0022112059000015

[31] Lourenco, L. M., and Krothapalli, A., "True Resolution PIV: A Mesh-Free Second Order Accurate Algorithm," *10th International Symposium on Applications of Laser Techniques to Fluid Mechanics*, Paper 13.5, July 2000.
[32] Lourenco, L. M., and Krothapalli, A., "Mesh Free Second Order Algorithm for PIV processing," *International Conference on Optical Technology and Image Processing in Fluid, Thermal and Combustion Flows*, Paper AB079, 1998.
[33] Lee, C., Hong, G., and Mallinson, S. G., "Influence of Synthetic Jet Location on Boundary Layer Separation Control," *Proceedings of the Device and Process Technologies for MEMS, Microelectronics, and Photonics III*, Vol. 5276, 1st ed., International Society for Optical Engineering, Bellingham, WA, 2004, pp. 230–239.
[34] Simpson, R. L., Chew, Y. T., and Shivaprasad, B. G., "The Structure of a Separating Turbulent Boundary Layer. Part 1. Mean Flow and Reynolds Stresses," *Journal of Fluid Mechanics*, Vol. 113, 1981, pp. 23–51. doi:10.1017/S002211208100339X
[35] Gorton, S. A., Owens, L. R., Jenkins, L. N., Allan, B. G., and Schuster, E. P., "Active Flow Control on a Boundary-Layer Ingesting Inlet," AIAA Paper 2004-1203, Jan. 2004.
[36] Viswanath, P. R., Ramesh, G., and Madhavan, K. T., "Separation Control by Tangential Blowing Inside The Bubble," *Experiments in Fluids*, Vol. 29, No. 1, 2000, pp. 96–102. doi:10.1007/s003480050431
[37] Johnston, J. P., and Nishi, M., "Vortex Generator Jets—Means for Flow Separation Control," *AIAA Journal*, Vol. 28, No. 6, 1990, pp. 989–994. doi:10.2514/3.25155
[38] Alvi, F. S., "The Role of Streamwise Vorticity in the Control of Impinging Jets," American Society of Mechanical Engineers Paper FEDSM2003-45062, July 2003.
[39] Marzouk, Y., and Ghoniem, A., "Vorticity Formulation for an Actuated Jet in Crossflow," AIAA Paper 2004-96, Jan. 2004.

N. Clemens
Associate Editor